Biological Trace Element Research (2020) 194:121–134
https://doi.org/10.1007/s12011-019-01742-2

Steering Efficacy of Nano Molybdenum Towards Cancer: Mechanism of Action

Janani Indrakumar[1] · Purna Sai Korrapati[1]

Received: 15 January 2019 / Accepted: 24 April 2019 / Published online: 23 May 2019

Abstract

Conventional cancer therapies possess a plethora of limitations which led to the awakening of nanotechnology and nanomedicine. However, technological success is widely dependent on complete understanding of the complexity and heterogeneity of tumor biology on one hand and nanobiointeractions associated with challenges of synthesis, translation, and commercialization on the other. The present study therefore deals with one such targeted approach aiming at synthesizing, characterizing, and understanding the efficacy of molybdenum oxide nanoparticles. The phase structure, morphology, and elemental composition of the synthesized nanoparticles were characterized using Fourier transform infrared spectroscopy, Raman spectroscopy, X-ray diffraction, X-ray photoelectron spectroscopy, and scanning electron microscopy. The cytotoxicity studies revealed that the IC_{50} vales of molybdenum trioxide (MoO_3) particles against skin cancer cells (melanoma and non-melanoma) were around 200–300 μg. The nanoparticles were found to induce mitochondrial-mediated apoptosis driven by the apoptotic genes such as BAX and Bcl_2. Molybdenum being a cofactor for the majority of metabolic enzymes could have triggered the selective internalization of the nanoparticles which in turn could have modified the granularity of the cytoplasm and subsequently lead to mitochondrial-mediated apoptosis. Further, the anti-angiogenic property of MoO_3 nanoparticles was corroborated using Chick chorioallantoic membrane (CAM) assay and aortic ring assay. Taken together , unraveling the role of MoO_3 nanoparticles in cancer and angiogenesis opens up venues for nano biological intervention of selective cancer cell targeting with minimal damage to the normal cells using natural trace elements that are generally known to influence various metabolic enzymes.

Keywords Metal oxide · Trace elements · Molybdenum · Cancer · Nanoparticle

Introduction

Nanomaterials with its awe-inspiring nanostructures have revamped the medical field owing to their plethora of inherent functional properties [1]. Among the various nanomaterials, nanoparticles have revolutionized modern therapeutics owing to their high specific surface area and inherent photocatalytic, optical, structural, mechanical, and magnetic properties in addition to their efficacy in permeability and retention. Further, unique features for drug delivery, diagnosis and imaging, synthetic vaccine development, and medical devices give promising hope for cancer. Cancer, a global life-threatening pathology, is scientifically defined as an uncontrolled proliferation and spread of abnormal cells. Tremendous efforts are being made in understanding its pathogenesis and developing drugs to combat cancer. In spite of enormous research, the high incidence rate and rapid recurrence make cancer a more challenging disease. Among other types, the prevalence of skin cancer is rapidly increasing due to cumulative exposure to adverse UV rays [2, 3]. Although skin cancer does not have any significant mortality rate, it is among the most commonly reported cancers all over the world. There are diverse types of skin cancers like basal cell carcinoma, squamous cell carcinoma, and melanoma. Melanoma cancers, in particular, have tendency to metastasize through regional lymph nodes to distant organs such as liver, lungs, and bone, and if metastasized, the probability of 5-year survival rate from diagnosis is reported to be decreased by 80% [4]. The present treatment strategies for skin cancer like radiation, chemotherapy, and surgery are plagued with side effects and unwarranted recurrences. Nanotechnology-based targeted drug delivery and therapeutic applications including diagnostic sensors and radiation

✉ Purna Sai Korrapati
purnasai@clri.res.in

[1] Biological Materials Laboratory, CSIR-Central Leather Research Institute, Adyar, Chennai, Tamil Nadu 600020, India

therapy are in vogue [5]. Nanoparticles, nanofibers, etc. have been used to deliver a variety of biomolecules and drugs to their target site [3–7]. In certain cases, the drugs themselves are also made into nanoparticles and are targeted to the required site [7]. The nanotechnological applications are widely used due to their high surface area to encapsulate the drug and extremely small size for easy penetration into the cell membrane [8]. Several reports on nanoparticles and its anti-cancer activity are available, but a lacuna is still present in developing an efficient mode of transport to carry the drug with minimal wastage and side effects arising due to unwanted drug leaching. Metal nanoparticles or metal oxide nanoparticles [9] such as Au [10], TiO_2 [11], ZnO [12], CeO_2 [13], and FeO [14] hold an important position in cancer therapeutics for their potential toxicity against cancer cells. They serve a major role in photothermal therapy and also help in targeting radiation towards the cancer cells [15]. Molybdenum, an essential trace element, serves as a cofactor for various enzymes such as xanthine dehydrogenase, aldehyde oxidase, sulfite oxidase, and nitrate reductase [16]. The permissible amount of molybdenum in circulation is 2 mg/day and complexes of molybdenum have also shown an anti-diabetic activity [17]. Molybdenum oxide has a strong localized surface plasmon resonance (LSPR) absorption in the near infrared region, which would enable them to play a major role in photothermal therapy for ablation of cancer cells [18]. Molybdenum oxide serves as a cheaper alternate for noble metals and has vital applications in cancer therapeutics. In nanoscale, its oxide form is non-toxic and safe when compared with other metal oxides [19]. Molybdenum trioxide (MoO_3) nanoparticles are reported to have an anti-microbial activity at minimal levels against *Staphylococcus aureus*, *Escherichia coli*, and *Pseudomonas aeruginosa* by activating membrane stress in the pathogen [20, 21]. Recently, these metal oxide nanoparticles are reported to induce significant toxicity towards invasive breast cancer cell lines. This paper essentially deals with unearthing the inherent potential of molybdenum oxide nanoparticles exhibiting selective cytotoxicity towards cancer cells through mitochondrial-mediated apoptotic pathway.

Experimental

Materials and Methods

All solvents used in this study were of analytical grade and were not further purified. Normal cell lines, HaCaT (keratinocytes), Swiss 3T3(fibroblasts), and cancer cell lines A431 (epidermoid carcinoma), HT1080 (fibrosarcoma), and G-361 (melanoma) were purchased from National Centre for Cell Science (NCCS), Pune, India. Cell culture medium and fetal bovine serum (FBS) were purchased from Life Technologies, USA. All the other chemicals used for the studies were procured from Sigma-Aldrich, India and were culture tested.

Nanoparticle Synthesis

Molybdenum trioxide nanoparticles were prepared as described by Krishnaswamy et al., with suitable modifications [22]. According to the procedure, 5 g of the precursor molybdic acid ($MoO_3 \cdot 2H_2O$) powder was calcined at 500 °C for 1 h in a furnace to yield molybdenum trioxide nanoparticles. The nanoparticles were allowed to cool down to room temperature and were stored in a sterile container until further usage.

Characterization of Nanoparticles

The surface morphology of the MoO_3 nanoparticles was analyzed by scanning electron microscopy (SEM) (Hitachi, Japan) using an accelerated voltage of 10 kV. The samples were gold sputter coated under argon atmosphere to make them electrically conductive preceding SEM analysis. The nature of the synthesized nanoparticles was analyzed by powder X-ray diffraction (XRD). The XRD patterns were evaluated using an X-ray diffractometer with CuKa radiation ($\lambda =$ 1.5405 Å) over a wide range of Bragg angles ($10° \leq 2\theta \geq 70°$). The scanning was carried out at 0.02 min^{-1} with a time constant of 2 s. The elemental composition of the nanoparticle after preparation was confirmed using X-ray Photoelectron Spectroscopic (XPS) studies. The XPS was performed using the instrument Axis Ultra DLD (Delay Line Detector) manufactured by Kratos Analytical.

Hemolysis Activity

Hemolytic assay was done according to the protocol reported by Sai *et.al* [20]. Briefly, 2 ml of blood was collected from a healthy individual rat in a heparinized vial and the red blood cells (RBCs) were isolated by centrifuging at 5000 rpm at 4 °C. The cells were washed thrice with warm HEPES buffer and approximately 10^8 RBCs (estimated based on OD value) were suspended in 1 ml of HEPES buffer containing the nanoparticles. The samples were incubated at 37 °C for 30 min and spun at 5000 rpm for 5 min. The supernatant was read at 540 nm in a microparticle reader (Bio-Rad Laboratories, USA).

Cell Culture

Human epidermal keratinocyte cell line (HaCaT), mouse embryonic fibroblasts (Swiss 3T3), and human squamous carcinoma (A431) cell lines were cultured in Dulbecco's modified Eagle's medium (DMEM: high glucose). Human fibrosarcoma (HT1080) and human skin malignant melanoma (G361) cell lines were cultured in (DMEM: low glucose) and

McCoy's medium, respectively. Human umbilical vein cell line (EA.hy926) was purchased from American Type Cell Culture (ATCC). The media were supplemented with 10% FBS and antibiotics streptomycin (100 μg/ml), penicillin (100 units/ml), gentamycin (30 μg/ml), and amphotericin B (2.5 μg/ml). The cells were maintained in 25-cm^2 culture flasks at 37 °C in a humidified incubator (Binder, Germany) supplied with 5% CO_2 and 95% air.

Cytotoxicity Studies

3-(4,5-Dimethylthiazol-2-yl)-2,5-diphenyltetrazoliumbromide (MTT) assay protocol [21] was followed to evaluate the cytotoxicity exhibited by the developed nanoparticles against cancer cells and normal cells. An equal density of 12×10^3 cells/well was seeded in a 48-well plate and left for attachment overnight. On the following day, cells were washed with PBS and treated with different concentrations of MoO_3 (50–400 μg) nanoparticles in triplicates. After 24 h of incubation, MTT (0.5 mg/ml in PBS) was added and incubated for 3 h at 37 °C. The formazan complex formed by the live cells was dissolved using DMSO and measured calorimetrically at 570/630 nm using a microplate reader (Bio-Rad Laboratories, USA).

Nanoparticle Uptake by Cells

The uptake of MoO_3 nanoparticles inside the cells and the change in the granularity of cells after treatment of MoO_3 nanoparticles were checked using flow cytometry BD FACSVerse. Equal density of 12×10^4 A431 cells was cultured in a 12-well plate and left for overnight attachment at 37 °C in a humidified incubator (Binder, Germany) supplied with 5% CO_2 and 95% air. On the following day, the cells were treated with IC_{50} concentration of MoO_3 nanoparticles. After 24-h incubation, the cells were trypsinized and were analyzed using a flow cytometer.

DNA Fragmentation

DNA fragmentation is one of the ideal experiments which shows the start and progress of apoptosis. Cells were treated with MoO_3 nanoparticles and incubated for 24 h in 37 °C in a humidified incubator (Binder, Germany) supplied with 5% CO_2 and 95% air. The cells were washed with PBS, fixed with 3% paraformaldehyde, permeabilized with 0.1% Triton X-100, and incubated with 0.5 μg/ml of 4′,6-diamidine-2′-phenylindole dihydrochloride (DAPI) for 10 min and observed under a fluorescence microscope (Leica Microsystems, Germany) to visualize the cell's morphology to confirm apoptosis.

Reactive Oxygen Species Generation

To estimate the generation of reactive oxygen species (ROS), A431 cells were seeded in a 12-well plate (40×10^3/well) and left for overnight attachment. On the following day, the cells were treated with IC_{50} concentration of MoO_3 nanoparticles and incubated for 4 h. After incubation, the cells were washed with PBS and incubated with 5 μM 2,7-dichloride dihydrofluorescein diacetate (DCFH-DA) in PBS for 30 min in the dark. After incubation, the cells were visualized in a fluorescence microscope filter (495 nm excitation and 523 nm emission) using Leica fluorescence microscope [22].

JC1 Staining

The mitochondrial membrane stability of the MoO_3 nanoparticle-treated cells was tested using JC1 dye. In the procedure, cells (40×10^3/well) were seeded in a 12-well tissue culture plate and left overnight at 37 °C in a CO_2 incubator. Cells were then treated for 24 h with MoO_3 nanoparticles followed by staining with 50 μM of JC1 dye for 30 min at 37 °C. The cells were then washed gently with warm PBS and images were captured using a fluorescence microscope (Leica Microsystems, Germany).

Flow Cytometry Analysis

A431 cells (1×10^6) were seeded on a 12-well tissue culture plate and left overnight in 37 °C in a humidified chamber with 5% CO_2 and 95% air for attachment. On the following day, the cells were treated with IC_{50} concentration of MoO_3 nanoparticles for about 16 h. After 16 h, the cells were trypsinized and suspended in 1X binding buffer containing Annexin and Propidium Iodide (PI) (sc-4253AK) according to manufacturer's protocol. The fluorescence exhibited by the cells was measured using a flow cytometer (BD FACSVerse, USA).

Gene Expression Studies

The expression of the apoptotic cascade induced due to the treatment of MoO_3 nanoparticles was analyzed by polymerase chain reaction (PCR). Total mRNA of the cells was isolated by treating the cells with MoO_3 nanoparticles for 24 h in 12-well particles. After 24 h, the RNA was isolated from the cells by using TRIzol reagent. The mRNA was converted into cDNA using PrimeScript RT Reagent Kit (Clontech Laboratories, USA). The converted cDNA was amplified using 2× REDTaq Ready Mix PCR reaction mix (Sigma-Aldrich) and gene-specific primers (Table 1). The PCR cycle conditions are mentioned below.

Table 1 PCR conditions

Condition	No. of cycles	Time	Temperature
Initial denaturation	35	3 min	95 °C
Melting temperature	35	30 s	Specific for primers (Table 2)
Extension	35	45 s	72 °C
Final extension		3 min	72 °C

Enzyme Linked Immunosorbent Assay

The A431 cells were cultured in a six-well plate and incubated with MoO_3 radioimmunoprecipitation assay buffer containing protease inhibitor cocktail (Sigma). The lysates were then centrifuged at 14,000×*g* for 15 min at 4 °C. The total protein from the supernatant was then subjected to bicinchoninic acid assay to determine the protein concentration. An equal amount of protein samples (20 μg/ml) was coated on a microtiter plate and allowed to incubate overnight at 4 °C. The coated plate was washed thrice with PBST, and the nonspecific protein binding sites were blocked by adding 200 μl of blocking buffer and incubated for 1 h at 37 °C. Primary antibodies of BAX (sc-7195), BCl_2 (sc-783), and β actin (sc-47778) were added in 1:1500 dilution and incubated for 2 h at 37 °C. The respective secondary antibodies, HRP conjugated goat anti-rabbit IgG HRP conjugated (sc-2030), and goat anti-mouse IgG HRP conjugated (sc-2005) were then added in 1:5000 dilution and incubated for 1 h at 37 °C. This was followed by the addition of 200 μl of TMB peroxidase substrate and peroxidase substrate mixed in the ratio 1:1, respectively, procured from Bethyl Laboratories (37-00-78) and incubated in the dark for about 30 min and the reaction was stopped by adding 50 μl of 2 N H_2SO_4. The absorbance was read at 405 nm in a microplate enzyme-linked immunosorbent assay (ELISA) reader (Bio-Rad, USA).

Angiogenesis

The major hallmark in the progression of cancer is tumor angiogenesis which is caused by the migration of endothelial cells towards the tumor to develop blood vessels. These blood vessels supply oxygen and nutrients to the growing carcinoma.

CAM Assay

In addition to apoptosis, angiogenesis plays a major role in tumor apoptosis. An effective anti-angiogenic moiety can prevent cancer from spreading from one organ to another. The anti-angiogenic efficacy of the MoO_3 nanoparticles was tested by using Chick chorioallantoic membrane (CAM) assay. Five-day-old fertilized eggs of white leghorn were used to test the anti-angiogenic characteristics of MoO_3 nanoparticles. The eggs were brought from Tamilnadu Egg Hatchery, Potherb, Kattankulathur, Kanchipuram and were sterilized on the surface using 70% ethanol. A small hole was drilled at the distal end of the eggs with the help of a sterile needle. This hole was made into a 2-cm^2 window for treating the nanoparticle. Whatman filter discs were soaked with 300 μg of MoO_3 nanoparticles and then carefully placed on chick chorioallantoic membrane. The open windows were then sealed with parafilm to prevent dehydration of the fluid and to avoid contamination. The eggs were placed at 37 °C in a humidified chamber (Binder, Germany). The parafilm was removed at periodic intervals and the angiogenic capillaries of the CAM were photographed with a digital camera.

Chick Aortic Ring Assay

To further confirm the anti-angiogenic activity of the MoO_3 nanoparticles, Chick aortic ring assay was performed. The eggs containing the embryo were cracked open and the embryos were transferred into a sterile Petri dish and dissected on the ventral side. Sprouting aorta was excised form 11-day-old fertilized chick embryo. The aorta was cut into fairly equal dimensions that is about 1–2 cm and was placed on collagen gel and MoO_3 containing collagen gel in a 24-well plate. The collagen gels were fibrillated and kept at 37 °C for 30 min. The collagen gel formed an extracellular matrix for the adherence and growth of the aorta. The matrix was supplemented with Dulbecco's modified Eagle's medium and the plate was incubated at 37 °C in a CO_2 chamber (95% air, 5% CO_2). The efficacy of the MoO_3 collagen in inhibiting angiogenesis was analyzed and recorded using a light microscope. After 72 h, the aorta was stained by calcein AM dye and photographed using a fluorescent microscope (Leica Microsystems, Germany).

Statistical Analysis

All the data that are mentioned in the paper are expressed as mean ± SD of three independent experiments. The results were expressed in mean and the standard deviation using Student's *t* test analysis. The data which was in the value $p < 0.05$ was considered to be statistically significant.

Results and Discussion

Scanning Electron Microscopy

MoO_3 is generally found to exist in three crystalline polymorphic forms, namely α orthorhombic, β monoclinic,

and hexagonal. However, the monoclinic and hexagonal are thermally unstable and thus the nanoparticles prepared by calcination of molybdic acid at 500 °C yielded the highly stable α orthorhombic nanoparticles. The SEM images shown in Fig. 1 clearly illustrate that the synthesized particles were in the form of a layered structure with a smooth surface. The synthesis methodology, calcination temperature, time, precursors, and other reaction parameters play a key role in the formation of structured particles. The nanoparticles were synthesized at different temperatures to standardize the ideal temperature for calcination of MoO_3 nanoparticles. These particles were also sonicated after subsequent calcination to yield spherical α orthorhombic MoO_3 nanoparticles. The formation of orthorhombic MoO_3 nanoparticles can be attributed to the layering of molybdic acid due to thermal treatment [22].

X-Ray Diffraction Spectroscopy

The nature of the MoO_3 nanoparticles and their purity were inferred using X-ray diffraction studies. The X-ray diffraction pattern (Fig. 2) signifies the structural formation of orthorhombic MoO_3 [23]. The peaks plotted from given 2θ values were in close correlation with reflection lines of α-MoO_3 (International Centre for Diffraction Data, Joint Committee on Powder Diffraction Standards, File No. 05-0508).

X-ray Photoelectron Spectroscopy

The formation of MoO_3nanoparticles was reconfirmed fusing X-ray photoelectron spectroscopy (XPS). The elemental fingerprint of a composite is established through XPS analysis. XPS was used to analyze the elemental composition of materials by irradiating them with a beam of X-rays and calculating the number of electrons that are excited. The full XPS spectra (Fig. 3a) for the nanoparticles showed prominent peaks corresponding to O1s, C1s, Mo3p, and Mo3d orbitals which validate the presence of elements molybdenum and oxygen in the formed nanoparticles. The deconvoluted spectra for molybdenum alone (Fig. 3b) showed peaks at 233 and 235 eV corresponding to Mo $3d_{3/2}$ and Mo $3d_{5/2}$, respectively. The spectra for oxygen (Fig. 3c) show peak at 530 eV [24]. The carbon element peaks which are generally obtained for correcting the accuracy of the obtained peaks are shown in Fig. 3d.

The Fourier infrared spectroscopy and the Raman spectroscopy were done to analyze the purity of the nanoparticle and have been reported in our previous study [25] conforming the synthesis of MoO_3 nanoparticles.

Hemolytic Assay

Hemolytic activity is a crucial factor that is required for therapeutic application, especially for metal-based nanoparticles as they have tendency to instigate a number of allergic immune reactions (Table 2). Hence, hemolytic

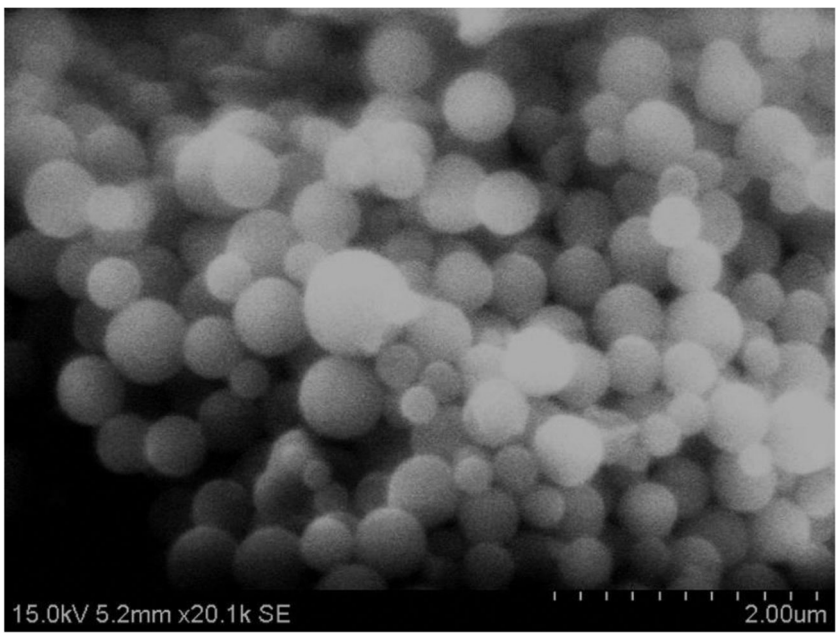

Fig. 1 SEM images of clusters of MoO_3 nanoparticles (scale bar 2 μm)

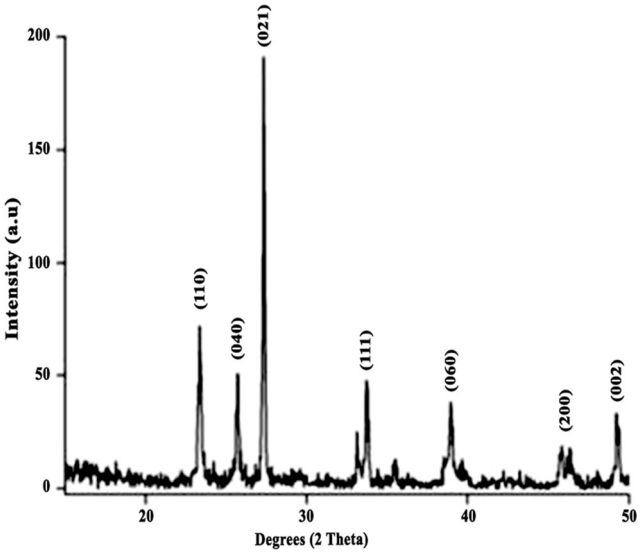

Fig. 2 XRD diffraction pattern of MoO_3 nanoparticles

compatibility for the given nanoparticle was tested using the hemolytic assay. The results were then tabulated in Table 3. Since water causes lysis of RBCs, water was used as the negative control, i.e., 100% hemolytic. MoO_3 nanoparticles also did not show any hemolysis which is on par with the previous reports on molybdenum [25]. This clearly shows that the fabricated nanoparticles will not elucidate any immune response in contact with the bloodstream.

Cytotoxicity

MTT assay is a standard test widely used to measure the toxicity of the prepared materials. The results of the MTT assay performed on different types of cancer cells and normal cells with varying concentrations of MoO_3 nanoparticles were illustrated in Fig. 4. All cells showed decreased cell viability with an increase in the concentration of nanoparticles. The percentage viability of the cells was calculated by considering the untreated control cells to be 100% viable and extrapolating the calculation to the treated cells. However, it was observed that at particular concentrations (200–300 μg/μl), the synthesized nanoparticles showed a decrease in more than 50% of the cell viability in melanoma and non-melanoma cells. The IC_{50} values for HaCaT and SWISS 3T3 were found to be around 400 μg in contrary to A431, HT1080, and G-361. This apparently reveals that MoO_3 nanoparticles show selective toxicity towards skin cancer cells.

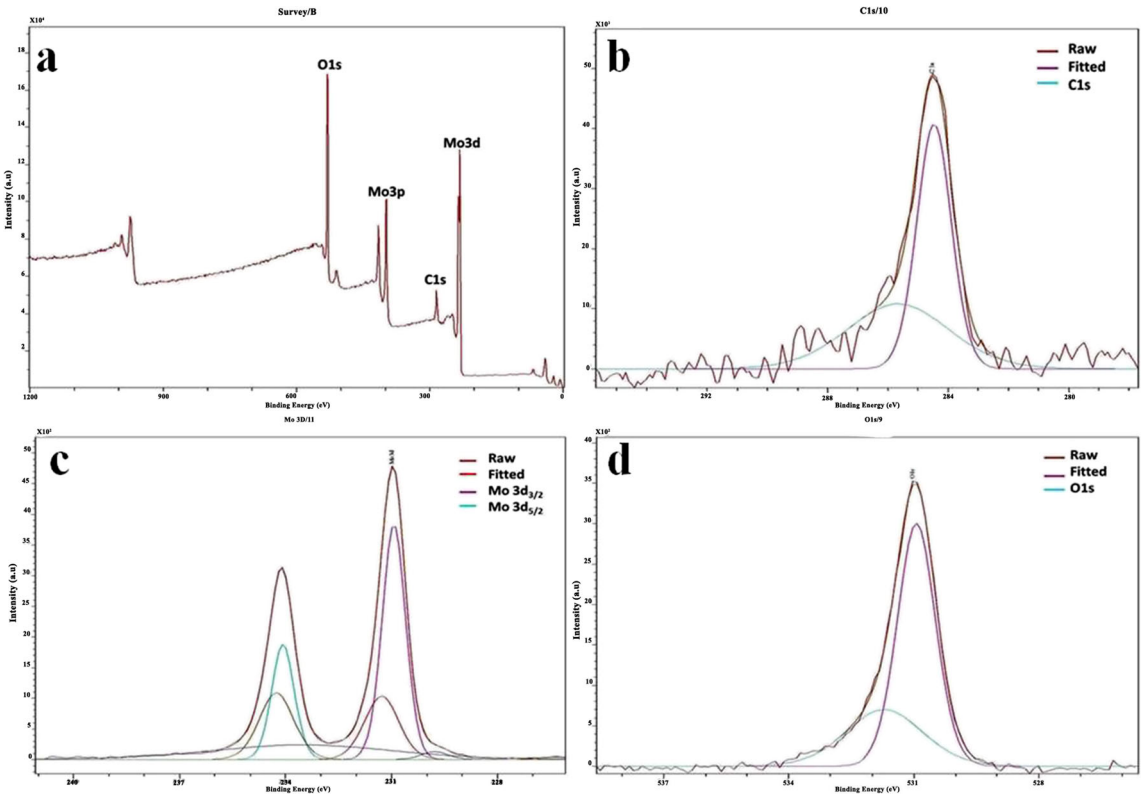

Fig. 3 X-ray photoelectron spectra of MoO_3 nanoparticles. **a** Full spectrum of MoO_3 nanoparticles. **b** Mo deconvoluted spectra. **c** O1s deconvoluted spectra. **d** C1s deconvoluted spectra Fourier transform infrared spectroscopy

Table 2 Percentage of hemolysis of the MoO_3 nanoparticles

Samples	% of hemolysis
Positive control	100
Negative control	0.03
MoO_3 NP (200 μg)	0.59 ± 0.067
MoO_3 NP (300 μg)	1.27 ± 0.063

Uptake of Nanoparticles by the Cells

The uptake of MoO_3 nanoparticles by A431 cells was monitored using flow cytometry. After incubating with MoO_3 nanoparticles for 24 h, the cells were trypsinized and analyzed using a flow cytometer. The side scatter of the cells was found to be higher after treating the cells with MoO_3 nanoparticles. The increase in granularity also signifies the entry of the nanoparticle into the cell Figure 5 indicates that there is a tremendous cell death observed in the nanoparticle-treated samples compared to the control confirming that the A431 cells are entering the cell death phase due to the internalisation of MoO3 nanoparticles

DNA Fragmentation

The beginning of apoptosis is generally characterized by fragmentation of the genomic DNA. MTT assay shows the cytotoxicity exhibited by the nanoparticles. Though the killing showed the toxicity of the nanoparticles, the mechanism of killing should be understood before regarding the molecule as a therapeutic molecule targeting cancer. DAPI is a stain that binds to A-T base pair of the DNA and emits blue fluorescence. A cell ready to undergo apoptosis exhibits chromatin condensation and fragmentation. The stained DNA becomes clearly visible due to the high florescence rendered by the distinct visible condensed chromatin network. Figure 6 clearly shows that the cells treated with the nanoparticles show fragmented and denatured DNA patterns which are visualized in a fluorescence microscope with DAPI staining. Hence, it is said that the cell might undergo apoptotic mode of cell death starting with DNA fragmentation.

Reactive Oxygen Species

ROS species involves a wide variety of radicals such as superoxide anion ($O2^-$), hydrogen peroxide (H_2O_2), hydroxyl radical (HO•), and singlet oxygen (1O2). All of which are more reactive than oxygen (O_2) itself. These molecules are majorly involved in the activation of the apoptosis cascade through mitochondria. The increasing ROS generation in a cellular system increases the oxidative damage to the cellular components and thereby pushes the cells to an apoptotic state [26]. Hence, the involvement of MoO_3 in ROS production is tested using a molecular probe DCFH-DA. DCFH-DA is a molecular probe that is permeable through the plasma membrane. This gets oxidized into DCF which emits fluorescence by the intracellular ROS that is present. Thereby, the greater the fluorescence is, the greater is the ROS present internally. Figure 7 shows the phase contrast and fluorescent microscopic images of control A431 cells and cells treated with IC_{50} concentration of MoO_3 nanoparticles. The presence of DCF is more prominent in the nanoparticle-treated cell lines. This concludes that the ROS generation was significantly higher in the A431 cells treated with MoO_3. This ROS produced subsequently causes the mitochondria to activate the apoptotic cascade.

Table 3 IC_{50} values of MoO_3 nanoparticles in different skin cancer cell lines

Cell line	IC_{50}
A431	296 ± 3.5 μg
HT1080	185 ± 4.7 μg
G-361	200 ± 7.8 μg

Mitochondrial Membrane Potential

Apoptosis in a cell can take place through either intrinsic pathway or extrinsic pathway. The intrinsic pathway is majorly initiated by the disruption of the mitochondrial membrane. Hence, to test the apoptotic pathway of the synthesized nanoparticle, JC-1 (5,5′,6,6′-tetrachloro-1,1′,3,3′-tetraethylbenzimidazol-carbocyanine iodide) was used to analyze the mitochondrial membrane potential of the treated and untreated samples. JC-1 is a cationic dye that gets aggregated in the mitochondria of live and healthy cells due to the intact mitochondrial membrane potential and gives a red color. Whereas, if there is any damage in the mitochondrial membrane, the polymer does not aggregate in the mitochondria but gets distributed in the cytoplasm as monomers which gives out green florescence [27]. Figure 8 signifies that the MoO_3 nanoparticle-treated cells emit a bright green fluorescence when compared to the control cells. The mitochondrial membrane potential dropped drastically in the MoO_3-treated cells, which caused the dye to exhibit itself in monomeric state. This clearly proves that the MoO_3 nanoparticles have caused mitochondrial membrane damage in the cultured A431 cell lines. This confirms the cytotoxicity towards cancer cells caused by MoO_3 due to mitochondrial membrane-mediated apoptosis of skin cancer cell lines.

Annexin-PI FACS

The mechanism of death induced by the MoO_3 nanoparticles was confirmed to be apoptosis by using flow

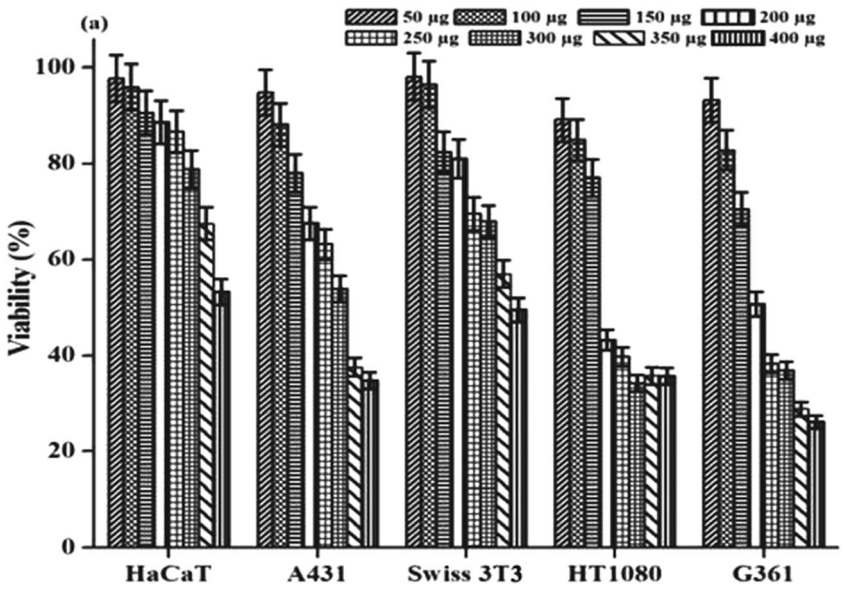

Fig. 4 Cytotoxicity caused by the MoO_3 nanoparticles

cytometry. During apoptosis, the cells exchange their peripheral phospholipid, i.e., phosphatidyl serine (PS), from the inner side of the cell membrane to the outer side exposing it to the extracellular space. Annexin V is a 35-kDa Ca^{2+}-dependent phospholipid binding protein which binds with PS but is incapable of entering the lipid bilayer (plasma membrane) when the cell is alive but when the cell is undergoing apoptosis, due to the flipping of PS from the inner side of the plasma membrane to the outer space causes interaction between Annexin (V) and PS. Annexin (V) is attached to the fluorescein isothiocyanate (FITC), an indicator for cells attached to Annexin (V) [28]. When the cells are stained with Annexin V-FITC and PI, they are subjected to falling: in the first quadrant are unstained cells, the second quadrant are early apoptotic cells (they are stained only by Annexin V-FITC), the third quadrant are late apoptotic cells (they are stained by Annexin V-FITC and PI, as their cell membrane and nuclear membrane are also compromised due to apoptosis), and the fourth quadrant are necrotic cells (the cells only stained with PI due to the loss of their cell membrane). Figure 9 shows the flow cytometry results of cells treated with IC_{50} concentration of MoO_3 nanoparticle. Since the MoO_3 nanoparticle was incubated for 16 h, the cells have reached an early apoptotic stage. As the incubation time increases, the cells will go to late apoptotic stage and then cell death. This quantitates the number of cells that undergo apoptosis after treating with MoO_3 nanoparticles.

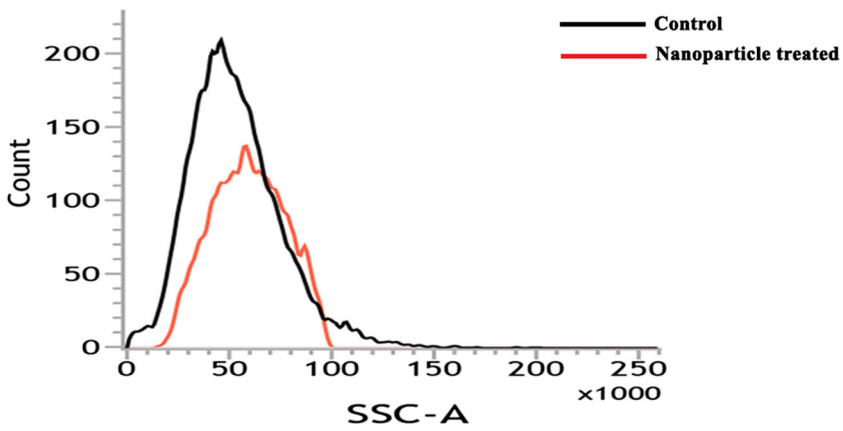

Fig. 5 MoO_3 nanoparticle uptake by A431 cells by flow cytometry

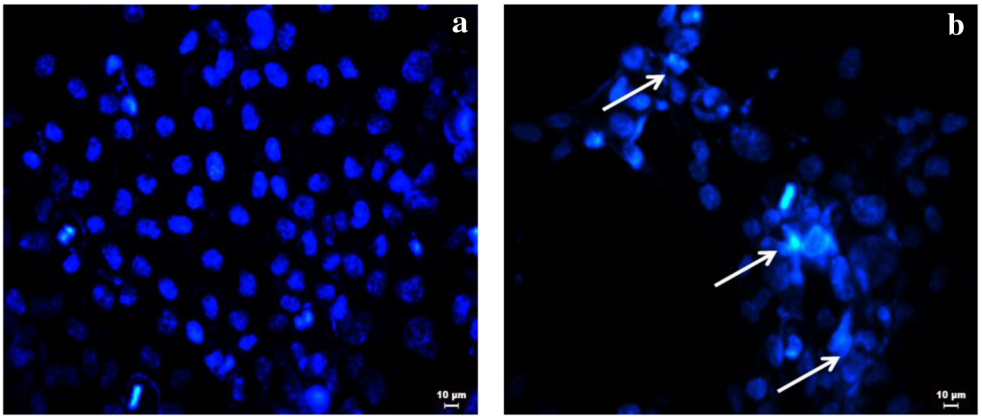

Fig. 6 DAPI-stained florescent microscope image of A431 cells. **a** Control. **b** Treated with IC_{50} concentration

Gene Expression Studies

The probable mechanism for mitochondrial-mediated apoptosis was investigated through PCR analysis and ELISA. The expression of apoptotic genes such as Bax, Bcl_2, and their protein expression was analyzed before and after treatment with IC_{50} concentration of the MoO_3 nanoparticles. It is evident from Fig. 10a that there is an increase in the expression of BAX genes and a decrease in Bcl_2 genes after treatment of A431 cell lines with MoO_3. The increase in the apoptotic protein and the decrease in the anti-apoptotic protein destabilize the mitochondrial membrane which in turn pushes the cell into apoptotic phase (Table 4). The corresponding protein expression also confirmed that the cell is entering apoptotic phase by activating the BAX-Bcl_2 pathway and represented in Fig. 10b.

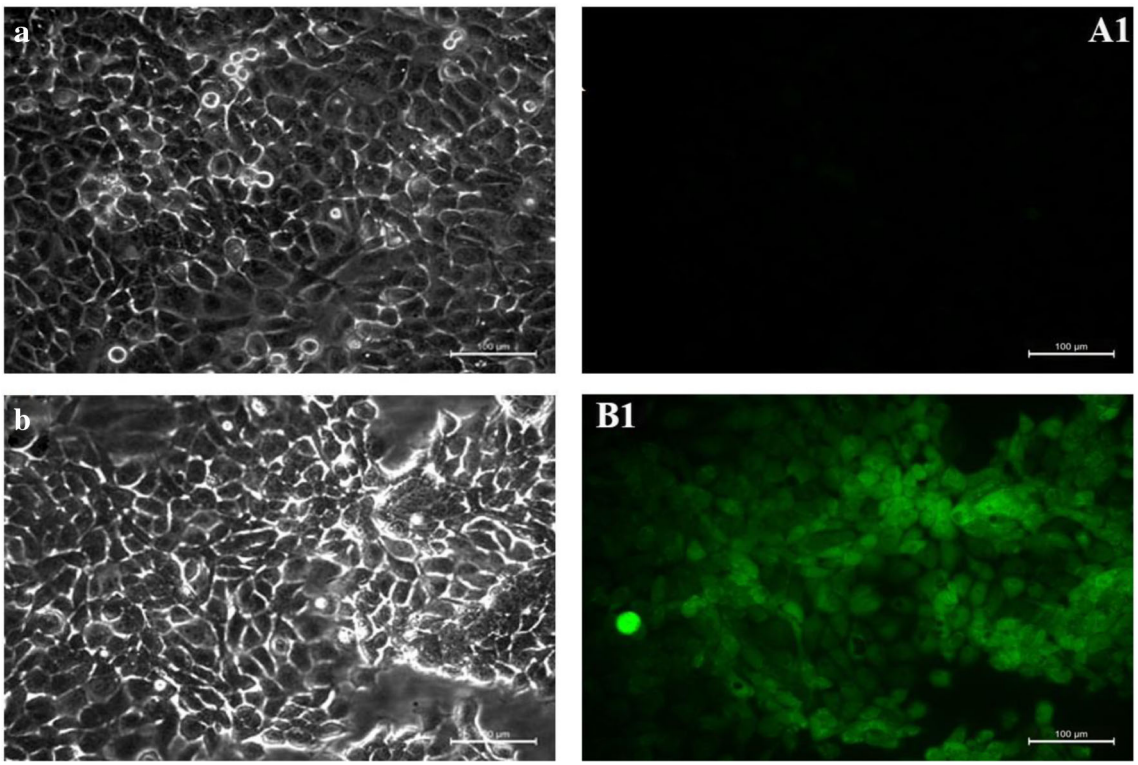

Fig. 7 Phase contrast microscopic images of A431 cells. **a** Control. **b** Treated with IC_{50} concentration of MoO_3 nanoparticle and fluorescence microscopic images of A431 cells. **A1** Control. **B1** Treated with IC_{50} concentration of MoO_3 nanoparticles

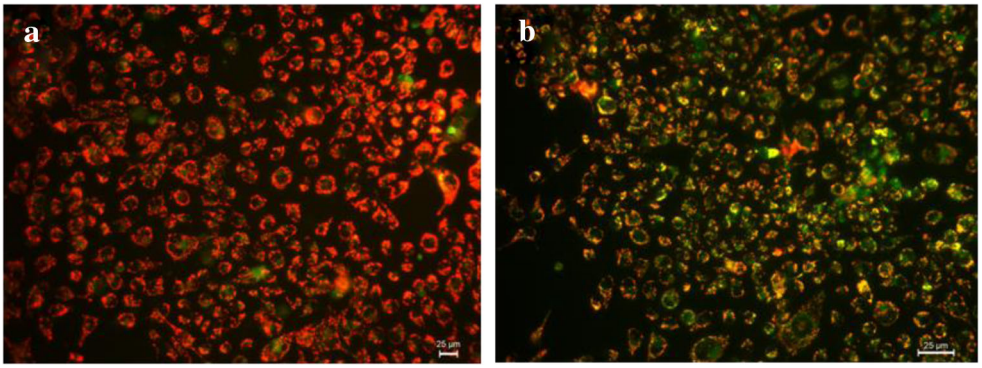

Fig. 8 JC-I-stained fluorescence microscope image of A431 cells. **a** Control. **b** Treated with IC_{50} concentration of MoO_3 nanoparticles

Angiogenesis

An important parameter of tumor progression is metastasis, which is responsible for cancer cell migration to different parts of the system. Angiogenesis plays a major role in growth and development of any tumor. In addition, it also forms a pathway for the tumor cells to travel to various organs and establish the tumor microenvironment. Hence, a molecule which kills cancer cells and also inhibits angiogenesis would serve as an ideal anti-cancer drug. Molybdenum salts are said to have anti-angiogenic properties in nature [29]. Molybdenum ions serve as an excellent chelating agent for copper, a cofactor for enzymes supporting angiogenesis [30]. Cu ions are also known to support proliferation and migration of endothelial cells [31]. Thus, the anti-cancer nature of MoO_3 nanoparticles was tested using various in vitro and in ovo experiments.

Endothelial Cell Migration

The main process of cancer progress is angiogenesis. The tumor mass which has developed harbors oxygen and nutrients for its development. The cancer cell thereby secretes a lot of cytokines that help in angiogenesis. Hence, a molecule that prevents the migration of endothelial cells and prevents angiogenesis can inhibit cancer prognosis. The ability of MoO_3 to hinder angiogenesis was tested using endothelial cell migration [32]. A wound created on the plate of EA.hy926 cells was treated with IC_{50} concentration of MoO3 nanoparticles and the migration of the cells to cover the wounded area was sequentially photographed using a light microscope at regular time intervals. From Fig. 11, it is evident that the wound created on the control EA.hy926 cells was almost closed at the end of the eighth hour, whereas the wound treated

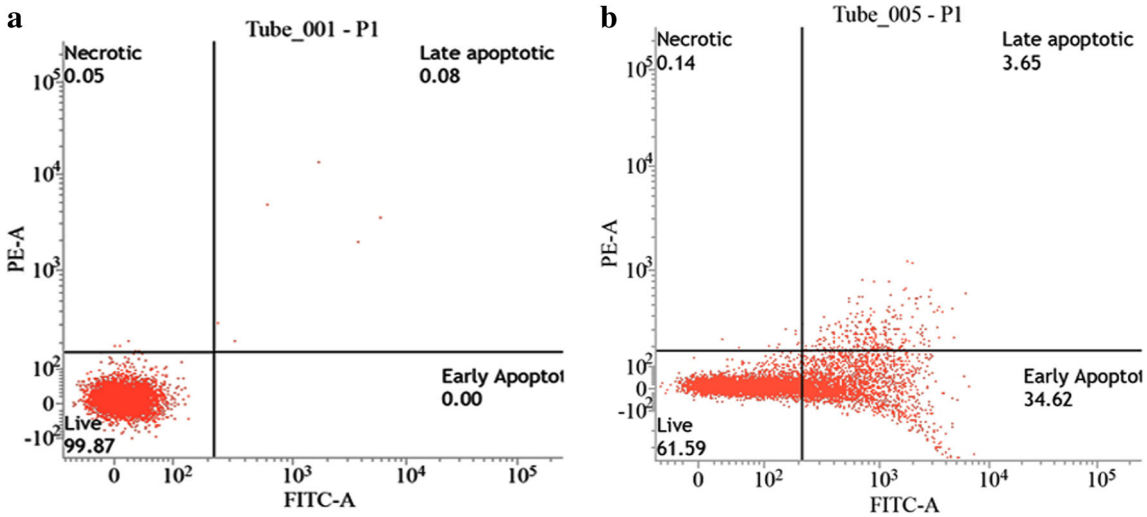

Fig. 9 Flow cytometry analysis using A431 treated with MoO_3 nanoparticles. **a** Control. **b** IC_{50} concentration of MoO_3 nanoparticles

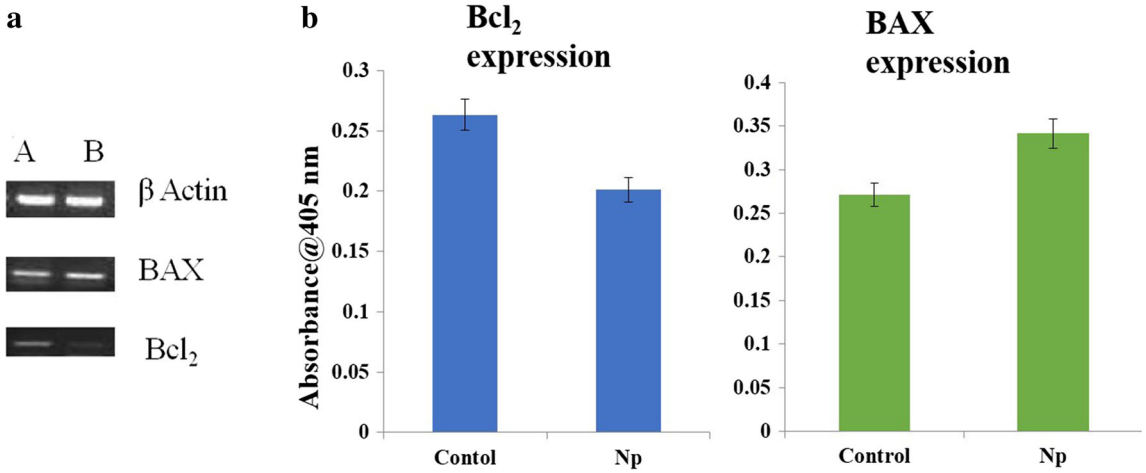

Fig. 10 **a** Gene expression of A431 cells (A) before treatment and (B) after treatment with IC_{50} concentration of MoO_3. **b** Protein expression of A431 cells

Table 4 Primer specification

Gene	Sequence	T_a (annealing temperature) in °C
BAX	5′ TGCTTCAGGGTTTCATCCA 3′ (Forward) 5′ GGCGGCAATCATCCTCTG 3′ (Reverse)	58
β-actin	5′TCACCACACCACTGTGCCCATCTACGA3′ (Forward) 5′AGCGGAACCGCTCATTGCCAATGG 3′ (Reverse)	60
Bcl_2	5′ AGGAAGTGAACATTTCGGTGAC 3′ (Forward) 5′ GCTCAGTTCCAGGACCAGGA 3′ (Reverse)	57

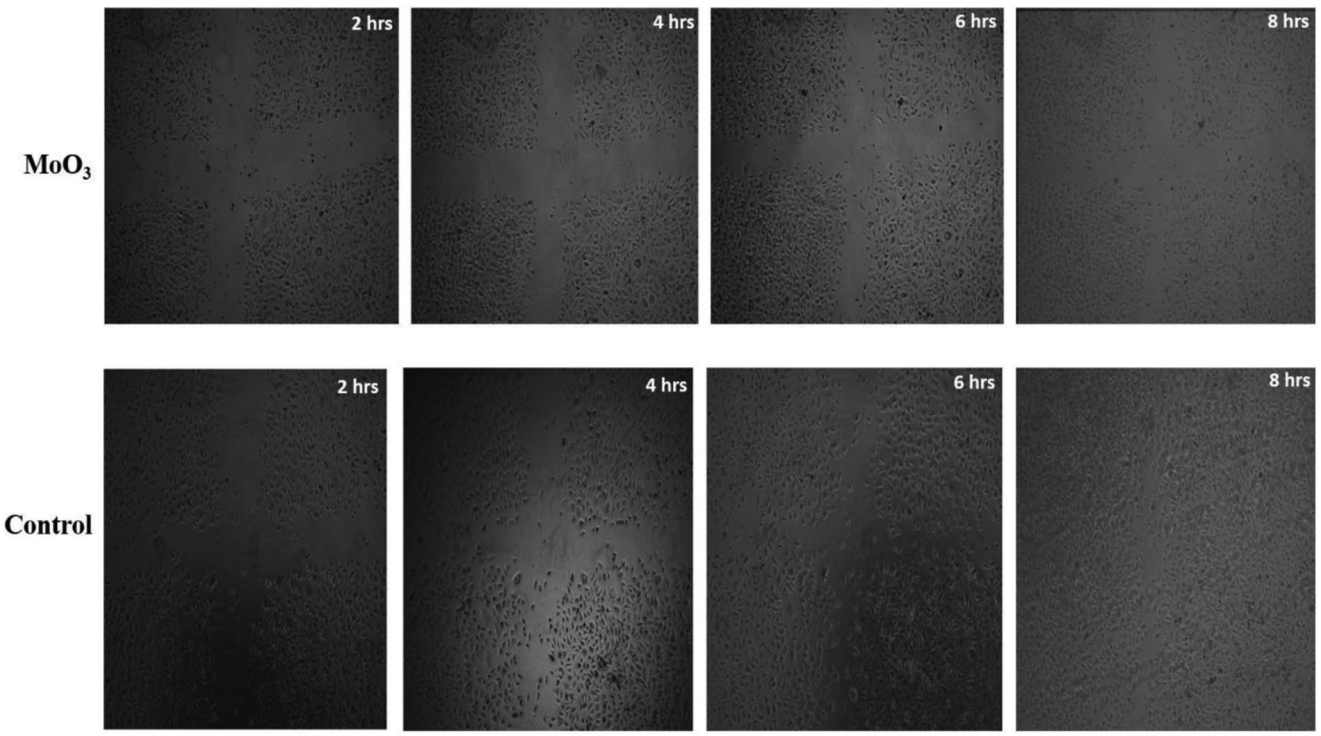

Fig. 11 Migration of EA.hy926 cells treated with MoO_3 nanoparticles

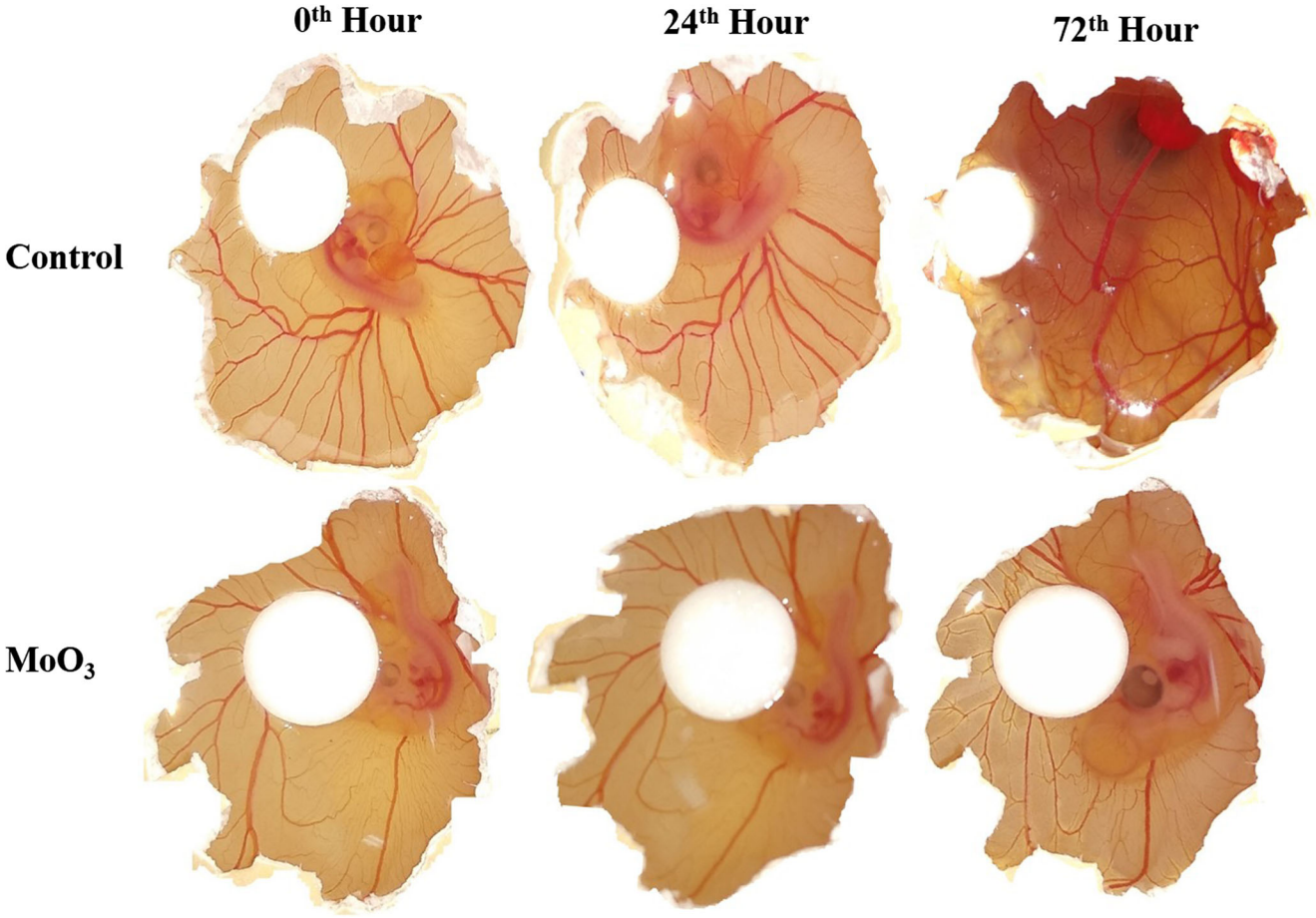

Fig. 12 Anti-angiogenic property of MoO_3 nanoparticles in CAM assay

with the MoO_3 nanoparticles prevented the closure of the abrasion, by inhibiting the migration of EA.hy926 cells. It could be seen from Fig. 11 that the EA.hy926 cells did not die but stopped migrating. This experiment proves that MoO_3 nanoparticles in addition to anti-cancer properties obstruct the migration of endothelial cells, restraining the development of nutritious blood vessels to the tumor tissue.

CAM Assay

Further, the anti-angiogenic property of MoO_3 nanoparticles was tested in ovo using CAM assay. The 3-day-old chicks were treated with MoO_3 nanoparticles and were observed for 72 h. Figure 12 clearly displays that the control samples showed good gradual development and thickening of capillaries marking the events of angiogenesis. Whereas the membranes treated with MoO_3 did not show any development or thickening of vessels [28]. The control samples showed an increase in the capillaries after 24 h. These capillaries thickened uniformly into prominent blood vessels after 72 h. In the CAM cultured with MoO_3 nanoparticles, there was no significant increase in the capillaries. This observation corroborated the *in vitro* endothelial migration experiment confirming the deterring role of MoO_3 in angiogenesis.

Chick Aortic Arch Assay

The chick aortic arch served as an *ex vivo* tissue model for assessing the anti-angiogenic trait of MoO_3 [33]. The budding pattern of the MoO_3-treated and untreated tissues is shown in Fig. 13. It is clearly manifested that the control aortic arch developed continuous microvessels in an orderly fashion. The aorta treated with MoO_3 nanoparticles showed very frail growth of vessels. At the end of 48^{th} hour, the aortic arch was stained with calcein AM dye and captured using a fluroscence microscope (Leica microsystems). The results elucidated that the control aorta shows a predominant growth and elongation of micro-blood vessels, while the nanoparticle-treated samples did not form any visible blood vessels. This experiment augments to the role of MoO_3 nanoparticles in inhibiting angiogenesis.

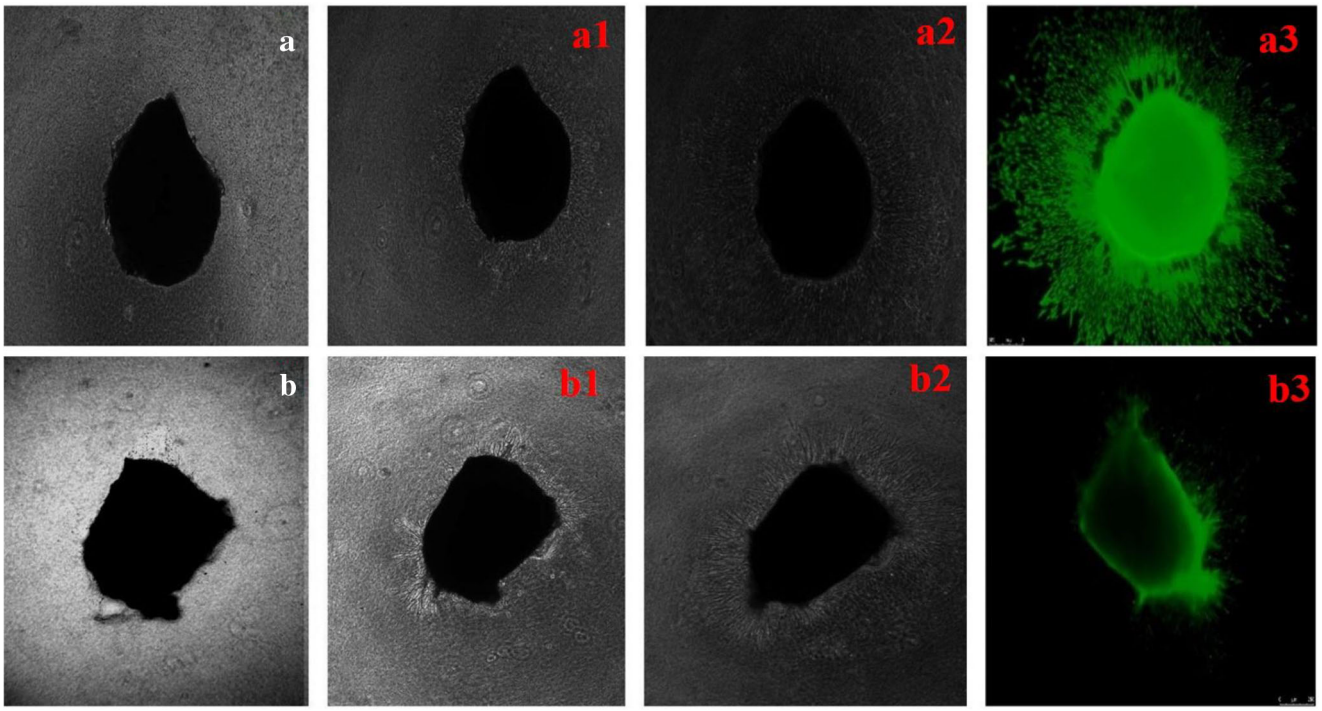

Fig. 13 Anti-angiogenic effect of MoO_3 nanoparticles represented by light microscopic images of sprouting chick aorta. Control aorta without treatment at **a** 0th hour, **a1** 24th hour, and **a2** 48th hour. Chick aorta treated with MoO_3 nanoparticles at **b** 0th hour, **b1** 24th hour, and **b2** 48th hour. Fluorescence microscopic images of calcein AM-treated control aorta (**a3**) and MoO_3-treated aorta (**b3**)

Conclusion

The synthesized MoO_3 nanoparticles exhibit an inherent cytotoxicity towards cancer cells in comparison to normal cells thereby serving as a target. Further, being a nanostructure also provides a scope for functionalizing and application as a targeted carrier for therapeutic agents for off-loading in cancer cells. In conclusion, this paper provides an insight to meet the challenges of controllable and reproducible synthetic strategies as well as facilitate the development of next-generation nanomedicine through incorporation of therapeutic bioactives/drugs reducing the limitations of drug payloads and resistance.

Acknowledgements The authors would like to acknowledge the ICMR for the financial support. The authors are also grateful to the Director, CSIR-CLRI, for his support and encouragement. The research work is carried out as a part of Ph.D. registered in the University of Madras.

Funding This study was funded by ICMR, India.

Compliance with Ethical Standards

Conflict of Interest The authors declare that they have no conflict of interest.

References

1. Li Z, Wang J, Li Y, Liu X, Yuan Q (2018) Self-assembled DNA nanomaterials with highly programmed structures and functions. Mater Chem Front 2:423–436. https://doi.org/10.1039/c7qm00434f
2. D'Orazio J, Jarrett S, Amaro-Ortiz A, Scott T (2013) UV radiation and the skin. Int J Mol Sci 14:12222–12248. https://doi.org/10.3390/ijms140612222
3. Harrison SC, Bergfeld WF (2009) Ultraviolet light and skin cancer in athletes. Sports Health 1:335–340. https://doi.org/10.1177/1941738109338923
4. Dianzani C, Zara GP, Maina G, Pettazzoni P, Pizzimenti S, Rossi F, Gigliotti CL, Ciamporcero ES, Daga M, Barrera G (2014) Drug delivery nanoparticles in skin cancers. Biomed Res Int 2014: 895986–895913. https://doi.org/10.1155/2014/895986
5. Conde J, Doria G, Baptista P (2012) Noble metal nanoparticles applications in cancer. J Drug Deliv 2012:1–12. https://doi.org/10.1155/2012/751075
6. Shoba E, Lakra R, Syamala Kiran M, Korrapati PS (2014) Design and development of papain/urea loaded PVA nanofibers for wound debridement.RSC Adv. 4:60209-60215. https://doi.org/10.1039/C4RA10239H
7. H.S.B.V.K.J, Basniwal NJRK (2011) Curcumin nanoparticles: preparation, characterization, and antimicrobial study. J. Food Agric. Chem 59:2056–2061
8. Pandurangan M, Nagajyothi PC, Shim J, Kim DH (2016) Antiproliferative effect of copper oxide nanorods against human cervical carcinoma cells. Biol Trace Elem Res 173:1–9. https://doi.org/10.1007/s12011-016-0628-0

9. Vinardell MP, Mitjans M (2015) Antitumor activities of metal oxide nanoparticles. Nanomaterials. 5:1004–1021. https://doi.org/10.3390/nano5021004
10. Rutberg FG, Dubina MV, Kolikov VA, Moiseenko FV, Ignat'eva EV, Volkov NM, Snetov VN, Stogov AY (2008) Effect of silver oxide nanoparticles on tumor growth in vivo. Dokl Biochem Biophys 421:191–193. https://doi.org/10.1134/S1607672908040078
11. Matsui K, Karasaki M, Segawa M, Hwang SY, Tanaka T, Ogino C, Kondo A (2010) Biofunctional TiO2 nanoparticle-mediated photokilling of cancer cells using UV irradiation. Medchemcomm. 1:209. https://doi.org/10.1039/c0md00027b
12. Rasmussen JW, Martinez E, Louka P, Wingett DG (2010) Zinc oxide nanoparticles for selective destruction of tumor cells and potential for drug delivery applications. Expert Opin Drug Deliv. 7: 1063-107. https://doi.org/10.1517/17425247.2010.502560
13. Sack M, Alili L, Karaman E, Das S, Gupta A, Seal S, Brenneisen P (n.d.) Combination of conventional chemotherapeutics with redox-active cerium oxide nanoparticles—a novel aspect in cancer therapy. Mol Cancer Ther.13:1740–1749. https://doi.org/10.1158/1535-7163.MCT-13-0950
14. Espinosa A, Di Corato R, Kolosnjaj-Tabi J, Flaud P, Pellegrino T, Wilhelm C (2016) Duality of iron oxide nanoparticles in cancer therapy: amplification of heating efficiency by magnetic hyperthermia and photothermal bimodal treatment. ACS Nano 10:2436–2446. https://doi.org/10.1021/acsnano.5b07249
15. Chithrani BD, Jelveh S, Jalali F, van Prooijen M, Allen C, Bristow RG, Hill RP, Jaffray DA (2010) Gold nanoparticles as radiation sensitizers in cancer therapy. Radiat Res 173:719–728. https://doi.org/10.1667/RR1984.1
16. Mendel RR, Bittner F (2006) Cell biology of molybdenum.Biochim Biophys Acta. 1763:621–635. https://doi.org/10.1016/j.bbamcr.2006.03.013
17. Levina A, McLeod AI, Seuring J, Lay PA (2007) Reactivity of potential anti-diabetic molybdenum(VI) complexes in biological media: a XANES spectroscopic study. J Inorg Biochem. https://doi.org/10.1016/j.jinorgbio.2007.07.016
18. Song G, Shen J, Jiang F, Hu R, Li W, An L, Zou R, Chen Z, Qin Z, Hu J (n.d.) Hydrophilic molybdenum oxide nanomaterials with controlled morphology and strong plasmonic absorption for photothermal ablation of cancer cells. 6:3915–3922. https://doi.org/10.1021/am4050184
19. Braydich-Stolle L, Hussain S, Schlager JJ, Hofmann M-C (n.d.) In vitro cytotoxicity of nanoparticles in mammalian germline stem cells. Toxicol Sci. 88:412–419. https://doi.org/10.1093/toxsci/kfi256
20. Sai KP, Jagannadham MV, Vairamani M, Raju NP, Devi AS, Nagaraj R, Sitaram N (2001) Tigerinins: novel antimicrobial peptides from the Indian frog Rana tigerina. J Biol Chem 276:2701–2707. https://doi.org/10.1074/jbc.M006615200
21. Mosmann T (1983) Rapid colorimetric assay for cellular growth and survival: application to proliferation and cytotoxicity assay. J Immunol Methods 65:55–63. https://doi.org/10.1016/0022-1759(83)90303-4
22. Krishnamoorthy K, Veerapandian M, Yun K, Kim J (2013) New function of molybdenum trioxide nanoplates: toxicity towards pathogenic bacteria through membrane stress. Colloids Surfaces B Biointerfaces 112:521–524. https://doi.org/10.1016/j.colsurfb.2013.08.026
23. Lackner M, Meier M, Shafaei S, Zollfrank C, Plank J, Guggenbichler JP (2013) Polymorphs of molybdenum trioxide as innovative antimicrobial materials. Surf Innov 1:202–208. https://doi.org/10.1680/si.13.00021
24. Xu Y, Zhang R, Huang L, Xu H, Li H, Xia J, Cheng X (2013) Synthesis and characterization of g-C3N4/MoO3 photocatalyst with improved visible-light photoactivity. Appl Surf Sci 283:25–32. https://doi.org/10.1016/j.apsusc.2013.05.106
25. Janani I, Lakra R, Kiran MS, Korrapati PS (2018) Selectivity and sensitivity of molybdenum oxide-polycaprolactone nanofiber composites on skin cancer: preliminary in-vitro and in-vivo implications. J Trace Elem Med Biol 49:60–71. https://doi.org/10.1016/j.jtemb.2018.04.033
26. Bai DP, Zhang XF, Zhang GL, Huang YF, Gurunathan S (2017) Zinc oxide nanoparticles induce apoptosis and autophagy in human ovarian cancer cells. Int J Nanomedicine 12:6521–6535. https://doi.org/10.2147/IJN.S140071
27. Wang J, Gao S, Wang S, Xu Z, Wei L (2018) Zinc oxide nanoparticles induce toxicity in CAL 27 oral cancer cell lines by activating PINK1/Parkin-mediated mitophagy. Int J Nanomedicine 13:3441–3450. https://doi.org/10.2147/IJN.S165699
28. Rajendran I, Dhandapani H, Anantanarayanan R, Rajaram R (2015) Apigenin mediated gold nanoparticle synthesis and their anticancer effect on human epidermoid carcinoma (A431) cells.RSC Adv. https://doi.org/10.1039/c5ra04303d
29. Munjal A, Vishwakarm P, Dhama K, Kujur A, Khandia R, Dwivedi A (2016) Molybdenum salts possess potent angiogenic modulatory properties: validation on chorioallantoic membrane (CAM) of chicken. Asian J Anim Vet Adv 12:44–49. https://doi.org/10.3923/ajava.2017.44.49
30. Micale N, Scarbaci K, Troiano V, Ettari R, Grasso S, Zappal M (2014) Peptide-based proteasome inhibitors in anticancer drug design.Med Res Rev. 30:1–69. https://doi.org/10.1002/med
31. Iakovidis I, Delimaris I, Piperakis SM (2011) Copper and its complexes in medicine: a biochemical approach. Mol Biol Int 2011:1–13. https://doi.org/10.4061/2011/594529
32. Poornima B, Korrapati PS (2017) Fabrication of chitosan-polycaprolactone composite nanofibrous scaffold for simultaneous delivery of ferulic acid and resveratrol. Carbohydr Polym 157: 1741–1749. https://doi.org/10.1016/j.carbpol.2016.11.056
33. Krishnaswamy VR, Balaguru UM, Chatterjee S, Korrapati PS (2017) Dermatopontin augments angiogenesis and modulates the expression of transforming growth factor beta 1 and integrin alpha 3 beta 1 in endothelial. Eur J Cell Biol 96:266–275. https://doi.org/10.1016/j.ejcb.2017.02.007